Croatian Society for Materials Protection

Metalurgija/Metallurgy

Vol. 66 No. 1 / 2026

Influence of Laser Shock Peening on the Corrosion and Corrosion Fatigue Behavior of 2Cr13 Martensitic Stainless Steel for Outdoor Piano

Dong Jiayin[1,*]

https://doi.org/10.64486/m.66.1.13

[1] Harbin University, Harbin City, No. 108, Sanfu Street, Xiangfang District, Harbin City, Heilongjiang Province, China, 150086

* Correspondence: 18445865202@163.com

Type of the Paper: Article

Received: April 20, 2026

Accepted: July 8, 2026

Abstract: The core metal components of outdoor pianos are exposed to complex natural environments such as rainwater and salt spray, and are prone to corrosion fatigue and pitting failure, which further leads to component performance degradation and shortened service life. In this paper, laser shock peening (LSP) technology was applied to perform surface modification on 2Cr13 martensitic stainless steel, which is commonly used in outdoor pianos. The effects of different peening parameters (energy and layer number) on the microstructure, mechanical properties and corrosion resistance of the material were systematically investigated. The results show that LSP can induce significant refinement of surface martensite laths, forming high-density dislocations and nanoprecipitates, with the surface microhardness increased by up to 44.1 %. In simulated outdoor environments with pH values of 3, 7 and 11, the corrosion fatigue crack growth rate was significantly reduced. In 3.5 % NaCl solution, the self-corrosion current density of the double-layer peened specimen decreased by 42.3 %. Through the synergistic effect of high-amplitude residual compressive stress and surface grain refinement, LSP effectively inhibits passive film breakdown and corrosion fatigue crack propagation.

Keywords: outdoor piano; 2Cr13 stainless steel; laser shock peening; corrosion fatigue; electrochemical corrosion

1. Introduction

With the rapid development of global public cultural infrastructure, outdoor pianos, as iconic facilities combining artistic value and public service functions, have been increasingly applied in urban parks, squares, campuses and tourist attractions. However, statistics show that the global annual economic loss caused by steel structure corrosion exceeds 2.5 trillion US dollars, of which corrosion damage to outdoor public facilities accounts for more than 15 % [1]. This work specifically targets the core load-bearing transmission components and exposed structural connectors in the action mechanism of outdoor pianos. These components are subjected to long-term repeated cyclic impact loads from keystroke operations while being directly exposed to harsh outdoor corrosive environments, and they are the critical failure parts that restrict the service life and operational stability of outdoor pianos. 2Cr13 martensitic stainless steel has become the mainstream material for the above-mentioned action components in commercial outdoor piano products. On one hand, it combines high strength, favorable hardness, excellent wear resistance and moderate manufacturing cost, which can fully meet the mechanical transmission requirements of long-term high-frequency keystroke operations. On the other hand, its inherent passivation characteristic provides basic corrosion resistance for general outdoor scenarios. However, under the coupled action of corrosive media and cyclic loads, its corrosion fatigue performance degrades significantly, which has become a prominent engineering pain point restricting the durability of outdoor pianos. This study addresses this practical demand. 2Cr13 martensitic stainless steel, however, has a relatively high carbon content, making it susceptible to pitting and intergranular corrosion in Cl^--containing environments. Moreover, under the synergistic effect of cyclic loading and corrosive media, the corrosion fatigue crack propagation rate increases exponentially.

Compared with conventional outdoor steel structures that mainly bear static or quasi-static loads, the service conditions of outdoor piano action components have distinct particularities. First, in terms of loading mode, the components withstand long-term high-frequency, low-amplitude cyclic impact loads from continuous keystrokes, forming a typical fretting-corrosion-fatigue coupling condition, which is essentially different from the load characteristics of ordinary outdoor building structures. Second, in terms of corrosion environment, in addition to conventional rain erosion, temperature-humidity alternation and salt spray corrosion, the components also face local condensation inside the semi-closed piano cavity and rapid temperature fluctuations caused by direct sunlight, forming a complex wet-dry alternating corrosion environment with wide pH fluctuation. Traditional anti-corrosion technologies for stainless steel mainly include surface coating, heat treatment and mechanical shot peening. Zamani et al. systematically compared the anti-corrosion properties of plasma-sprayed Al_2O_3, Cr_2O_3 and their composite coatings on carbon steel, and found that the composite coating reduced the corrosion current density by more than 40 % compared with single coatings, but the bonding strength between the coating and the substrate was only (20–30) MPa, making it prone to cracking and peeling under cyclic loading [2]. Early research by Zhu et al. showed that tempering temperature had a significant effect on the stress corrosion cracking susceptibility of 2Cr13 stainless steel, and the material exhibited the best stress corrosion resistance when tempered at 600°C. However, heat treatment introduces residual tensile stress on the material surface, which accelerates crack initiation [3]. Topic et al. found that cold working and heat treatment altered the fatigue behavior of 3CR12 corrosion-resistant steel wire, and the fatigue life decreased by more than 50 % when the cold working rate exceeded 30 % [4]. Maher et al. pointed out in a review that traditional anti-corrosion technologies cannot effectively solve the synergistic failure problem of wear and corrosion, while outdoor piano components are subjected to both cyclic loading and corrosive media simultaneously, and a single anti-corrosion measure often fails to achieve the expected effect [5].

Laser shock peening (LSP), as a novel non-contact surface modification technology, induces GPa-level high-pressure shock waves on the material surface through high-energy pulsed lasers, causing severe plastic deformation in the surface layer and generating high-amplitude residual compressive stress and nanocrystalline structures. It has become a research hotspot in the field of stainless steel corrosion protection. Sundar et al. systematically summarized the principles, processes and applications of laser shock peening technology in a review, pointing out that this technology has been industrialized in aerospace and marine engineering fields, and its strengthening effect is 3–5 times that of traditional shot peening [6]. In terms of electrochemical corrosion protection, Wei et al. first systematically studied the effect of laser shock peening on the electrochemical corrosion resistance of AISI 304 stainless steel in acidic chloride solution, and found that laser shock peening reduced the self-corrosion current density by more than 35 % and significantly increased the pitting potential [7]. Lu et al. further investigated the effect of different pulse energies on the corrosion behavior of 304 stainless steel, and found that the corrosion rate decreased by 62 % as the pulse energy increased from 3 J to 7 J, confirming the regulatory effect of energy parameters on the strengthening effect [8]. Nataraj et al. developed a coating-free laser peening process, which avoids surface contamination caused by absorption layer residues while maintaining a strengthening effect comparable to traditional processes, expanding its application in precision components [9]. Liu et al. applied this technology to 316L stainless steel welded joints and found that laser shock peening effectively eliminated residual tensile stress in the weld zone, reducing the self-corrosion current density of the weld zone by 53 % [10]. Li et al. further extended laser shock peening technology to zirconium alloy surfaces, and found that it reduced the corrosion rate of zirconium alloy in high-temperature and high-pressure water by 47 %, proving the universality of this technology [11]. Okonkwo et al. recently compared the long-term corrosion behavior of two 304 stainless steels in boron-lithium containing high-temperature water, revealing the influence mechanism of alloying elements on passive film stability [12]. Choudhary et al. further revealed the origin mechanism of passive film breakdown and metastable pitting in 316L stainless steel at the atomic scale, pointing out that laser shock-induced grain refinement can increase the enrichment of Cr elements in the passive film, thereby significantly improving its pitting resistance [13].

In the field of corrosion fatigue protection, laser shock peening has also made important progress. Luo et al. studied the effect of laser shock peening with different coverage layers on the fatigue performance of Fe-Cr alloy in NaCl solution, and found that 2-layer peening increased the corrosion fatigue life by more than 40 %, and the strengthening mechanism was mainly attributed to the synergistic effect of residual compressive stress and grain refinement [14]. Recent research by Deng et al. focused on 2Cr13 martensitic stainless steel and systematically analyzed the effect of coverage layers on fatigue crack initiation and propagation, finding that the crack propagation rate decreased by 38 % as the coverage layer increased from 1 to 3 [15]. Wang et al. found that laser shock-induced surface gradient stress distribution effectively prolonged the corrosion fatigue life of AISI 420 stainless steel, and the life extension mechanism was closely related to the stress shielding effect at the crack tip [16]. Sheng et al. investigated the effect of laser non-uniform shock peening on the fatigue performance of 304 stainless steel welded joints, and found that non-uniform shock produced a more reasonable residual stress distribution, increasing the fatigue life of welded joints by 52 % [17]. Rubio-Gonzalez et al. compared the effects of laser shock peening and traditional shot peening on fatigue crack propagation in duplex stainless steel, and found that laser shock peening was more than 45 % effective than traditional shot peening [18]. Liao et al. revealed the dislocation pinning effect induced by nano-precipitates during laser shock peening through dislocation dynamics simulation and experimental verification, which is an important microscopic mechanism for improving material strength and fatigue performance [19]. Zhuang et al. successfully applied laser shock peening technology to aero-engine compressor rotor blades, increasing their fatigue life by more than 3 times, fully demonstrating the engineering practicability of this technology [20].

Despite significant progress in laser shock peening (LSP) technology for stainless steel corrosion protection, existing studies still have notable limitations: they mainly focus on extreme service environments such as aerospace and marine engineering, and lack targeted research on the coupled corrosion environment characterized by wide pH fluctuations, high Cl^- concentration gradients and low-cycle cyclic loading, which is typical for civilian equipment. For 2Cr13 martensitic stainless steel, most relevant studies are limited to single fatigue or static corrosion properties, failing to deeply reveal the synergistic damage mechanism between electrochemical corrosion and corrosion fatigue. Furthermore, no LSP process parameter system suitable for such service conditions has been established, making it difficult to directly guide engineering applications. To address these gaps, this paper takes 2Cr13 martensitic stainless steel commonly used in outdoor equipment as the research object, adopts LSP processes with different laser energies and peening layers, and systematically investigates the influence of LSP parameters on the corrosion resistance of the material in simulated outdoor corrosion environments through microstructural characterization, electrochemical corrosion tests, corrosion fatigue tests and finite element numerical simulation, and deeply reveals its strengthening mechanism. The research results can provide theoretical basis and experimental support for the corrosion protection design and process optimization of metal components in civilian equipment, including outdoor pianos.

2. Materials and Methods

2.1. Experimental Materials and Specimen Preparation

The experimental material was standard 2Cr13 martensitic stainless steel for outdoor piano metal components, with its chemical composition (mass fraction, %) shown in Table 1. The material was supplied in the annealed state, with mechanical properties: tensile strength 640 MPa, conditional yield strength 440 MPa,

https://doi.org/10.64486/m.66.1.13

elongation 20 %. The substrate pretreatment process was as follows: Stainless steel plates with a thickness of 2 mm were cut into 30 mm × 30 mm × 2 mm specimens by wire electrical discharge machining (WEDM), totaling 12 pieces, which were divided into 3 groups for later use. Then, one surface of each specimen was ground smooth with 100# to 2000# sandpapers, ultrasonically cleaned with alcohol and dried. The central 25 mm × 15 mm area of the specimen surface was designated as the laser shock peening area.

Table 1. Chemical composition of 2Cr13 stainless steel / wt. %

Stainless Steel	C	Si	Mn	P	S	Cr	Cu	Fe
2Cr13	0.20	0.45	0.41	0.021	0.060	12.61	0.12	Balance

2.2. Laser Shock Peening Process

2.2.1. Microstructure and Surface Properties

2Cr13 martensitic stainless steel plates with a thickness of 2 mm were processed into 30 mm × 30 mm × 2 mm specimens by wire electrical discharge machining (WEDM). A total of 12 specimens were prepared and equally divided into 3 groups for subsequent experiments. One surface of each specimen was sequentially ground to a smooth finish using 100# to 2000# metallographic sandpapers, followed by ultrasonic cleaning in anhydrous ethanol and cold air drying. A central region of 25 mm × 15 mm on the specimen surface was selected as the laser shock peening (LSP) treatment area.

The LSP experiments were performed using a YS80-M165 LSP complete system (Xi'an Tianruida Optoelectronic Technology Co., Ltd.). The main technical parameters of the system are as follows: maximum output energy of 8 J (continuously adjustable), pulse width of (18–20) ns, focused spot diameter of (2–5) mm, positioning accuracy of the six-axis robot of ±0.2 mm, processing frequency of (1–10) Hz, and laser wavelength of 1064 nm. The system is equipped with a water nozzle robot that can cooperate with the six-axis robot to apply the water confinement layer.

Two groups were subjected to single-layer and double-layer LSP treatments, designated as LSP-1 and LSP-2 groups, respectively; the remaining group served as the untreated control group. The LSP process parameters were set as: pulse energy of 7.6 J, spot diameter of 3 mm, spot overlap rate of 50 %, and processing frequency of 8 Hz. Black adhesive tape was used as the absorbing protective layer, and running water was used as the confinement layer. For double-layer treatment, the black adhesive tape was replaced after each layer of impact, and residual tape on the specimen surface was removed upon completion of all treatments.

2.2.2. Corrosion Fatigue Resistance

Double-sided sequential laser shock peening (LSP) was performed on the specimens, with a central 12 mm × 12 mm area selected as the impact region. Black adhesive tape was used as the absorbing protective layer, and running water served as the confinement layer. Specimens in groups S1, S2 and S3 were treated with single energy of 7.6 J, single energy of 5.6 J, and gradient energy of 7.6 J-5.6 J-3.6 J, respectively. During the LSP process, specimens were clamped by a CNC manipulator to complete the strengthening treatment on the front and back surfaces sequentially. After the impact, residual black adhesive tape on the specimen surface was removed, and the specimens were ultrasonically cleaned in acetone solution for subsequent tests.

All three-point bending fatigue specimens were divided into 4 groups according to the impact process: Group 1 was the untreated control group (6 specimens), Group 2 was the S1 group (treated with 7.6 J, 6 specimens), Group 3 was the S2 group (treated with 5.6 J, 2 specimens), and Group 4 was the S3 group (treated with 7.6 J-5.6 J-3.6 J gradient energy, 2 specimens).

2.2.3. Electrochemical Corrosion

Two types of specimens were prepared for electrochemical corrosion experiments: 6 untreated substrate specimens with dimensions of 10 mm × 10 mm × 4 mm, and 10 specimens with dimensions of 16 mm × 16 mm × 4 mm subjected to laser shock peening (LSP) treatment with three different process parameters, namely 7.6 J

 https://doi.org/10.64486/m.66.1.13

single-layer impact (labeled as 7.6 J-1), 5.6 J single-layer impact (labeled as 5.6 J-1), and 7.6 J double-layer impact (labeled as 7.6 J-2). The impact area of all LSP specimens was the central 12 mm × 12 mm region on the upper surface.

The general process parameters of the LSP experiments were as follows: pulse duration of 18 ns, wavelength of 1064 nm, spot diameter of 3 mm, and spot overlap rate of 50 %. A flowing water layer with a thickness of 1 mm was used as the transparent confinement layer, and black adhesive tape was used as the absorptive protective layer. The black adhesive tape was replaced after each layer for multi-layer impact. After all impacts were completed, the residual black adhesive tape on the specimen surface was removed, and the specimen surface was ultrasonically cleaned with acetone.

2.3. Performance Testing Methods

Microstructure characterization: Metallographic structures were observed using a LEICA DM2500M optical microscope with an etchant of 93 % alcohol + 7 % nitric acid solution. Surface microstructures were analyzed using a JEM-2100 high-resolution transmission electron microscope (HRTEM) at an accelerating voltage of 200 kV.

Mechanical property testing: Microhardness was measured using an HXD-1000TMSC/LCD microhardness tester with a load of 400 gf and a holding time of 10 s. Five points were measured on each specimen and the average value was taken. Surface roughness (Ra) was measured using an Axio CSM 700 confocal microscope, with three areas measured on each specimen and the average value taken.

Corrosion fatigue testing: A MTS810 electro-hydraulic servo fatigue testing machine was used, with triangular wave loading, a frequency of 8 Hz, a maximum load of 3 kN, and a stress ratio of R = 0.1. The corrosive media were 3.5 % NaCl solutions with pH values of 3, 7, and 11, respectively, to simulate the corrosive environments of acid rain, neutral rainwater, and alkaline condensation encountered during actual outdoor service, covering the typical pH fluctuation range inside the piano cavity. The crack length was monitored in real time using the compliance method. After the experiments, fracture morphologies were observed, and EDS energy spectrum analysis was performed using a JSM-6700F scanning electron microscope (SEM).

Electrochemical corrosion testing: A CHI760E electrochemical workstation was used with a three-electrode system (working electrode: 2Cr13 stainless steel specimen, auxiliary electrode: platinum sheet, reference electrode: saturated calomel electrode). The corrosive media were NaCl solutions with mass fractions of 3.5 %, 7 %, and 10 %, which were selected to simulate the corrosion intensity differences under different outdoor exposure scenarios, such as inland low-salt areas, coastal salt spray areas, and high-concentration salt accumulation in local areas. The test contents included: open circuit potential (OCP, test time 800 s), potentiodynamic polarization curve (scanning range −1.5 V to −0.5 V, scanning rate 0.005 V/s), and electrochemical impedance spectroscopy (EIS, test frequency range 0.01 Hz to 10^5 Hz, AC voltage amplitude 10 mV).

3. Results and Discussion

3.1. Effect of Laser Shock Peening on Microstructure and Mechanical Properties

The effect of laser shock peening on the microstructure of 2Cr13 stainless steel is shown in Figure 1. The unpeened specimen exhibited a typical coarse and straight martensite lath structure with large grain size (Figure 1a). After 1-layer laser shock peening, the martensite laths were significantly refined and the lath spacing decreased (Figure 1b). After 2-layer peening, the refinement effect was further enhanced, and subgrain structures formed in some regions (Figure 1c). This is because the high-pressure shock waves generated by laser shock peening cause severe plastic deformation in the material surface layer, inducing the generation of a large number of dislocations which interweave to form dislocation walls and dislocation cells, eventually developing into subgrain boundaries and grain boundaries, and decomposing the original coarse martensite laths into fine grains.

 https://doi.org/10.64486/m.66.1.13

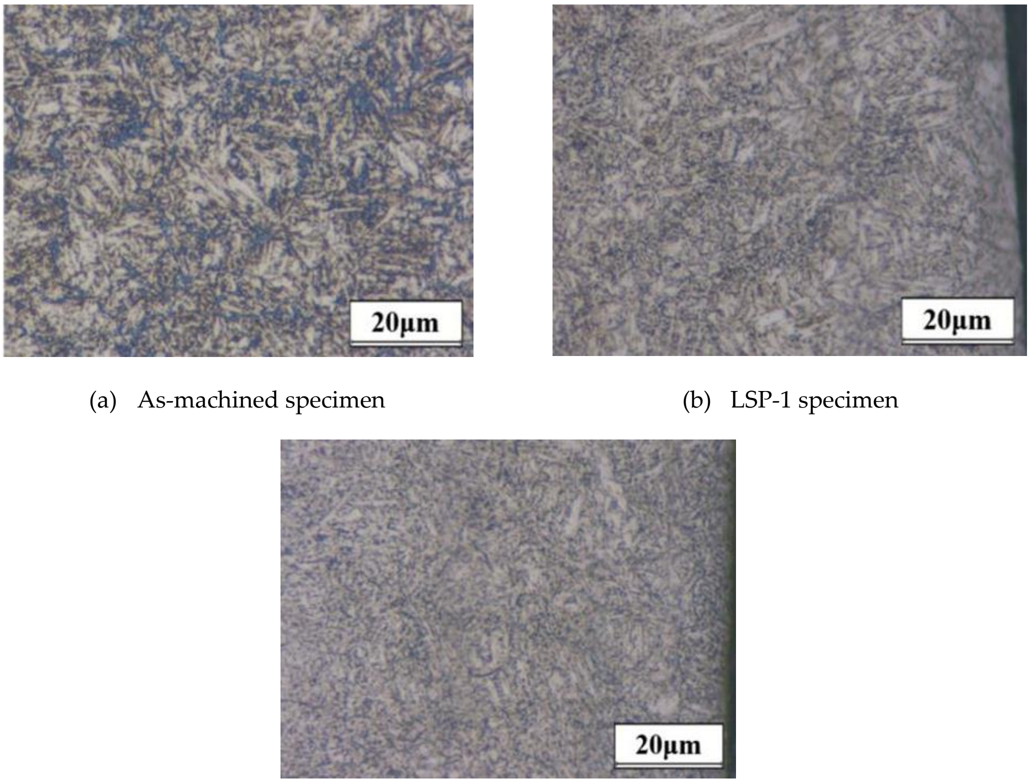

(a) As-machined specimen (b) LSP-1 specimen

(c) LSP-2 specimen

Figure 1. Surface metallographic structures of different specimens

Characterization and analysis of microstructures, especially the surface dislocation configurations, are critical means to reveal the laser shock peening (LSP) mechanism and correlate the microstructures with macroscopic mechanical properties of materials. In this section, transmission electron microscopy (TEM) was employed to characterize the surface microstructures of 2Cr13 stainless steel, and the dislocation configurations and microstructure evolution of the specimen surfaces before and after LSP treatment were systematically analyzed. Figure 2 shows the TEM morphology of the untreated 2Cr13 stainless steel specimen. The untreated specimen exhibits coarse and elongated martensite laths arranged approximately in parallel, with dislocation pile-ups and tangles inside the laths. A large number of coarse carbides precipitate at the martensite lath boundaries, which are presumed to be products of the prior mechanical processing. These carbides cause local Cr depletion, reducing the corrosion resistance of the material and serving as preferential sites for crack initiation.

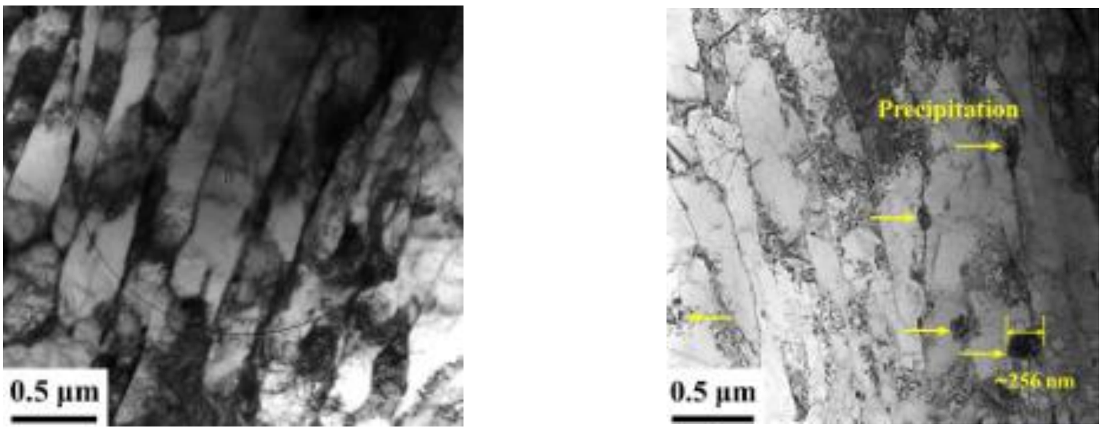

(a) Martensitic lath (b) precipitation

Figure 2. TEM images of as-machined specimen

 https://doi.org/10.64486/m.66.1.13

Figure 3 presents the TEM morphology of the LSP-1 specimen. After single-layer LSP treatment, high-density dislocations are formed in the specimen surface layer, and typical substructures such as dislocation lines, dislocation walls and dislocation cells evolve. This is attributed to the severe plastic deformation induced by high-energy laser pulses on the target surface, which leads to significant refinement of the surface microstructure. As shown in Figure 3(c), a large number of discontinuous strip-shaped nanoprecipitates are precipitated at the martensite boundaries. These nanoprecipitates can hinder dislocation movement through the dislocation pinning effect, thereby activating new dislocation sources and multiplying dislocations [47]. Since 2Cr13 stainless steel has a body-centered cubic (BCC) structure, its plastic deformation is mainly dominated by slip. The hindrance of dislocation slip significantly improves the mechanical properties of the material, delays the initiation of fatigue cracks, and enhances its corrosion resistance.

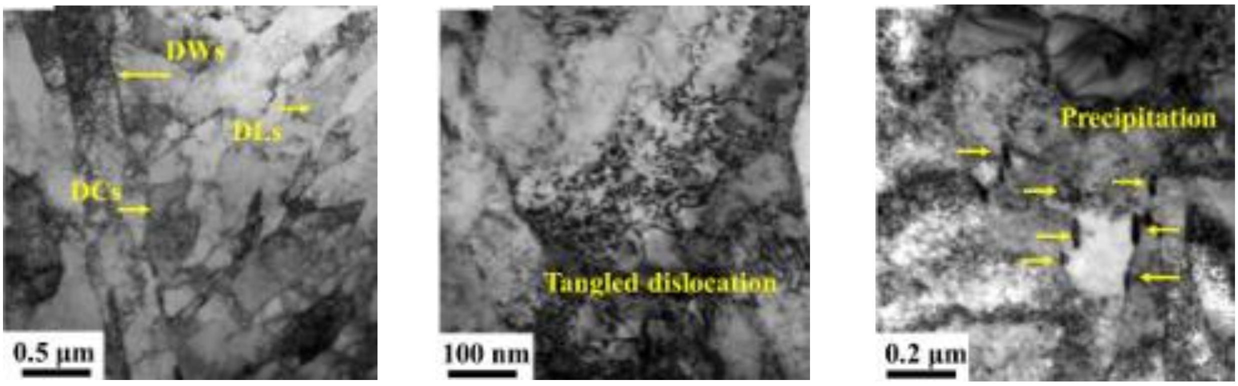

(a) Martensitic lath (b) tangled dislocation (c) strip precipitation

Figure 3. TEM images of LSP-1 specimen

Figure 4 illustrates the TEM morphology of the LSP-2 specimen. After double-layer LSP treatment, the refinement degree of martensite laths is further improved, and high-density dislocation tangles are formed. Compared with the LSP-1 specimen, the dislocation configuration of the LSP-2 specimen is more stable, and subgrain structures are formed. A large number of nanoprecipitates are precipitated in the dislocation tangle regions. The high-density nanoprecipitates not only hinder dislocation movement, but also dislocation pile-ups provide new precipitation sites for the nanoprecipitates. The synergistic effect between them further improves the mechanical properties of the material. By comparing Figure 2 and Figure 3, it can be seen that the composite structure of nanoprecipitates and interwoven dislocations formed in the surface layer of the LSP-2 specimen is more stable than that of the LSP-1 specimen. This indicates that with the increase of LSP layers, the surface grains of the material are further refined, the mechanical properties are continuously improved, and the corrosion resistance and fatigue resistance are also enhanced.

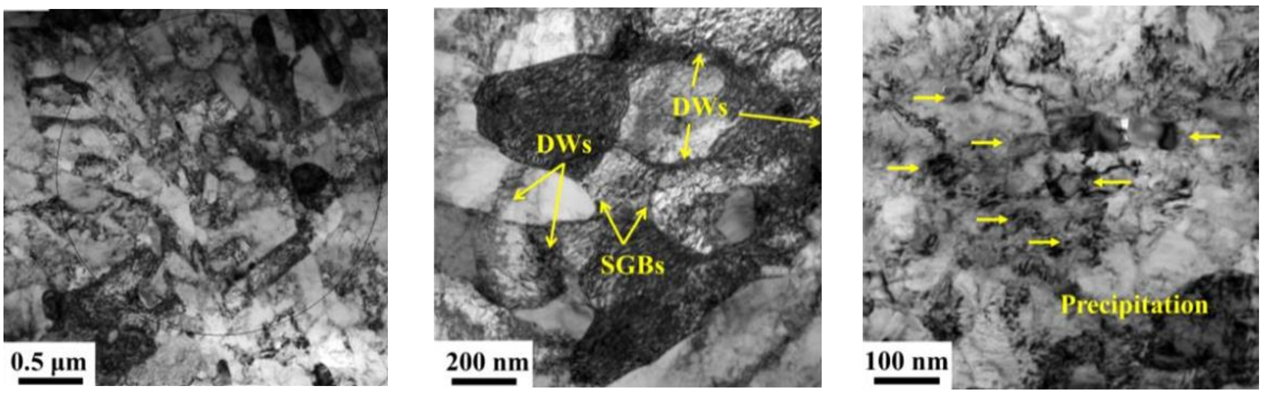

(a) Martensitic (b) Dislocation (c) Precipitation

Figure 4. TEM images of LSP-2 specimen

https://doi.org/10.64486/m.66.1.13

The microhardness and surface roughness of specimens under different peening parameters are shown in Table 2. The results show that microhardness increased significantly with the increase of peening layers. The microhardness of the unpeened specimen was 263 HV, and that of LSP-1 and LSP-2 specimens increased by 31.2 % and 44.1 %, respectively. The improvement in hardness is mainly attributed to the synergistic effect of grain refinement strengthening and dislocation strengthening. Higher hardness means better wear resistance and deformation resistance of outdoor piano components, which can reduce surface defects caused by wear and thus lower the probability of corrosion initiation. Meanwhile, surface roughness increased with the increase of peening layers, which is caused by the uniform plastic deformation of the material surface forming pits due to laser shock. Although the increase in surface roughness will increase the adsorption area of corrosive media to a certain extent, the positive effects of residual compressive stress and grain refinement brought by laser shock peening far outweigh the negative effects of roughness. The significant improvement in surface microhardness can directly enhance the wear resistance and deformation resistance of outdoor piano action components under long-term high-frequency keystroke friction, reduce surface wear defects that act as preferential initiation sites for corrosion pits and fatigue cracks, and lay a foundation for extending the service life of components.

Table 2. Microhardness and surface roughness of specimens under different laser shock peening parameters

Stainless Steel	Specimen	Microhardness HV	Standard deviation / HV	Improvement rate / %	Surface roughness Ra / μm
2Cr13	Unpeened	263	5	-	0.23
-	LSP-1	345	8	31.2	0.51
-	LSP-2	379	10	44.1	0.69

3.2. Effect of Laser Shock Peening on Corrosion Fatigue Performance

The a-N curves of unpeened specimens and three laser shock peened specimens (S1, S2 and S3) in NaCl solutions with different pH values are shown in Figure 5. The initial total crack length was 8 mm, including 2 mm pre-crack and 6 mm WEDM notch length. The results show that laser shock peening significantly improved the corrosion fatigue life of 2Cr13 stainless steel, and the life improvement was proportional to the peening energy. In NaCl solution with pH=7, the fatigue cycle number of the unpeened specimen was 41897, while those of S1, S2 and S3 specimens were 48217, 45851 and 47619, respectively, corresponding to life improvements of 15.08 %, 9.44 % and 13.66 % compared with the unpeened specimen. It is worth noting that the life difference between S3 (gradient peening) and S1 specimens was not significant, indicating that the effective action area of laser shock peening is mainly concentrated at the crack tip. This finding has important guiding significance for engineering applications, meaning that only laser shock peening on the stress concentration areas of components can achieve significant strengthening effects, thereby reducing processing costs.

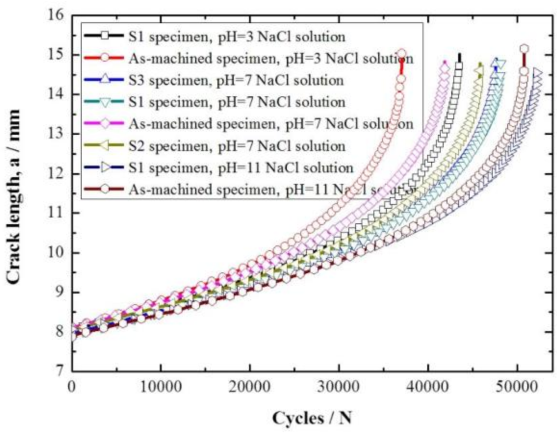

Figure 5. α -N curves of specimens with different peening energies in NaCl solutions with different pH values

 https://doi.org/10.64486/m.66.1.13

The pH value of the corrosive solution had a significant effect on fatigue life. For the unpeened specimen, the life at pH = 3 decreased by 11.55 % compared with that at pH=7, while the life at pH=11 increased by 21.31 %. For the S1 specimen, the fatigue cycle numbers at pH = 3 and pH = 11 were 43546 and 52257, respectively, showing the same trend as the unpeened specimen. This is because hydrogen evolution corrosion occurs in acidic environments, and hydrogen atoms penetrate into the material interior causing hydrogen embrittlement, which accelerates crack propagation; while oxygen absorption corrosion occurs in alkaline environments, and the formed Cr_2O_3 protective film is more stable. The largest life improvement of laser shock peened specimens was observed in acidic environments, indicating that this technology can effectively inhibit hydrogen-induced cracking, and is especially suitable for outdoor pianos in acid rain-prone areas.

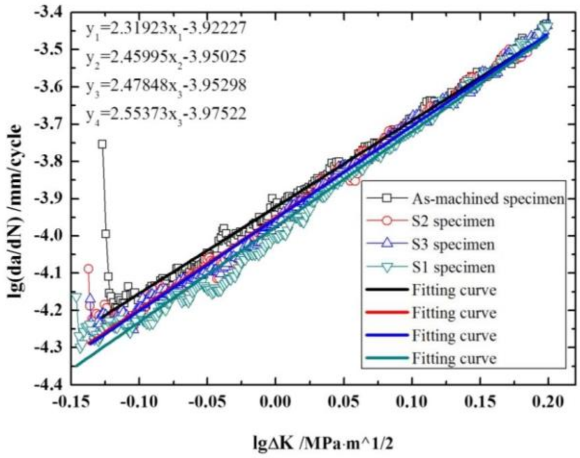

Figure 6. lg(da/dN)-lg(ΔK) curves of different specimens in NaCl solution with pH = 7

The corrosion fatigue crack growth rates of the four types of specimens were fitted using the Paris formula, with the fitting equation being lg(da/dN) = lg(C) + lg(ΔK). The corresponding material constants C and m for each group were calculated accordingly. In NaCl solution at pH = 7, the C values of the untreated, S1, S2 and S3 specimens were -3.92227, -3.97522, -3.95025 and -3.95298, respectively, and the m values were 2.31923, 2.55373, 2.45995 and 2.47848, respectively, as shown in Figure 3.

The experimental results show that after laser shock peening (LSP) treatment, the m value of the specimens increases significantly and exhibits an increasing trend with rising impact energy, while the material constant C decreases significantly and exhibits a decreasing trend with rising impact energy. When the stress intensity factor ΔK was 0.781, the da/dN values of the untreated, S1, S2 and S3 specimens were 6.78×10^{-5}, 5.53×10^{-5}, 6.25×10^{-5} and 5.73×10^{-5}, respectively. This indicates that under the same ΔK condition, the corrosion fatigue crack growth rates of all LSP-treated specimens are lower than that of the untreated specimen. Among them, the S1 specimen has the lowest growth rate, the S3 specimen is slightly higher than S1, and the S2 specimen shows the smallest reduction amplitude.

The underlying mechanism is as follows: LSP can introduce high-amplitude residual compressive stress into the material surface layer, and the stress amplitude is positively correlated with the impact energy. In the initial stage of crack growth, the incompletely released residual compressive stress can effectively inhibit the propagation of corrosion fatigue cracks. However, with the increase of ΔK, the crack propagates continuously, the residual compressive stress is gradually released and finally approaches zero, and the strengthening effect of LSP weakens accordingly, thus leading to a gradual increase in the crack growth rate. A higher impact energy introduces a larger amplitude of residual compressive stress into the specimen surface layer, resulting in a more significant reduction in the crack growth rate. Since the residual compressive stress is gradually released as the crack propagates, the inhibitory effect of LSP on corrosion fatigue cracks is mainly concentrated in the crack tip region.

The surface residual stress distributions of specimens before and after corrosion fatigue tests are shown in Figure 4. Before the test, the maximum surface residual compressive stress of the unpeened specimen was -

 https://doi.org/10.64486/m.66.1.13

305 MPa (generated by machining), while those of S1 and S2 specimens reached -588 MPa and -506 MPa, respectively, proportional to the peening energy. The residual stress of S3 specimen showed a gradient distribution along the crack propagation direction, with higher energy regions corresponding to higher residual compressive stresses. After the test, the residual compressive stresses of all specimens were significantly released with crack propagation, and basically disappeared in the crack propagation region, and even residual tensile stresses appeared in the final fracture region. This further proves that the effect of residual compressive stress is mainly reflected in the crack initiation and low-speed propagation stages. As the crack continues to propagate, the residual compressive stress is gradually consumed, and its strengthening effect weakens accordingly. The reduction of corrosion fatigue crack growth rate and the extension of fatigue life mean that under the same outdoor service conditions, the maintenance cycle of outdoor piano transmission components can be significantly prolonged, and the risk of sudden fracture failure of components is reduced, effectively improving the long-term operational reliability of outdoor pianos. In addition, the finding that the strengthening effect of LSP is mainly concentrated at the crack tip provides a cost-saving idea for engineering applications: targeted LSP treatment only on stress concentration areas of components can achieve satisfactory strengthening effects.

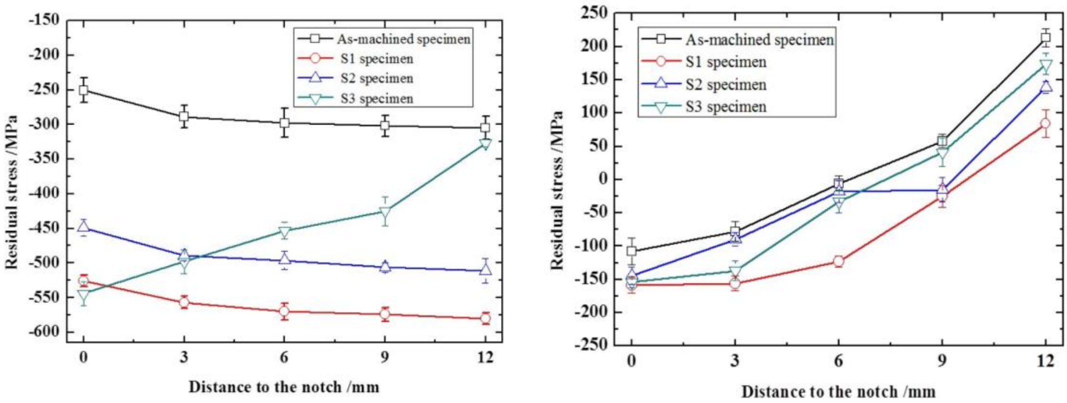

(a) Before CFCG test (b) After CFCG test

Figure 7. Surface residual stresses for as-machined and three kinds of LSPed specimens

3.3. Effect of Laser Shock Peening on Electrochemical Corrosion Performance

Figure 8 shows the potentiodynamic polarization curves of the untreated and laser shock peened (LSP) specimens with different process parameters in 3.5 wt. % NaCl solution. The polarization curve of 2Cr13 stainless steel exhibits the typical self-passivation characteristics of passive metals with a distinct passivation plateau, indicating its certain resistance to Cl^- corrosion[55]. In NaCl solution, a passive film spontaneously forms on the material surface. When the applied potential exceeds the pitting potential, the passive film breaks down, pitting initiates, and the current density increases sharply.

The self-corrosion potentials of the untreated, 5.6 J-1, 7.6 J-1 and 7.6 J-2 specimens were obtained by fitting curves a to d, which were -1.046 V, -1.012 V, -1.007 V and -0.967 V, respectively. The results show that after LSP treatment, the self-corrosion potential of the specimens shifts positively, the polarization curve moves toward lower current densities as a whole, and the pitting potential increases simultaneously, confirming that laser shock peening can significantly improve the electrochemical corrosion resistance of 2Cr13 stainless steel.

Further analysis of the corrosion current density reveals that both the self-corrosion current density (icorr) and passivation current density of the LSP-treated specimens are significantly reduced. With the increase of LSP impact energy and number of impact layers, the positive shift amplitude of the self-corrosion potential increases, and the reduction amplitude of the self-corrosion current density becomes more significant. This indicates that within the experimental parameter range of this study, increasing the impact energy or the number of impact layers can further improve the corrosion resistance of 2Cr13 stainless steel, and the strengthening effect of double-layer impact is better than that of single-layer impact.

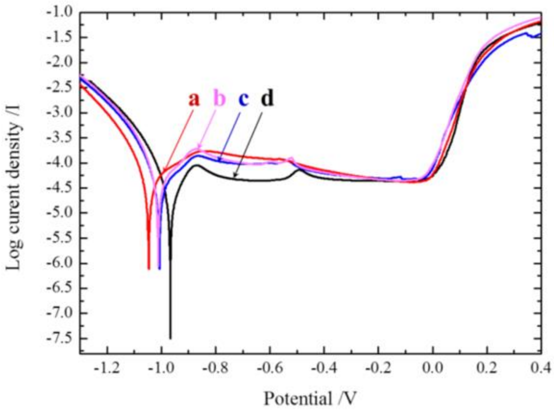

Figure 8. Polarization curves of different specimens in 3.5 % NaCl solution(a) Unpeened specimen; (b) 5.6 J-1 specimen; (c) 7.6 J-1 specimen; (d) 7.6 J-2 specimen

Figure 9 shows the potentiodynamic polarization curves of the untreated 2Cr13 stainless steel specimens in NaCl solutions with different mass fractions. The self-corrosion potentials (Ecorr) in 3.5 %, 7 % and 10 % NaCl solutions were -0.856 V, -0.964 V and -0.999 V, respectively. With the increase of NaCl concentration, the self-corrosion potential of the specimens shifted negatively gradually. Among them, the passivation region was the widest in 3.5 % NaCl solution, indicating that the passive film formed under this condition had the best stability. The above results show that the increase of Cl^- concentration accelerates the dissolution of the passive film on the surface of 2Cr13 stainless steel, leading to the decrease of its corrosion resistance.

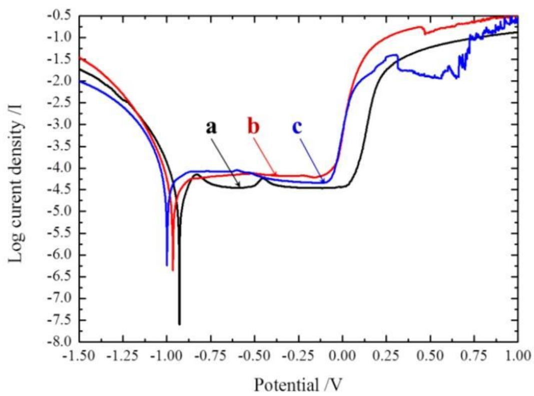

Figure 9. Polarization curves of unpeened specimen in NaCl solutions with different concentrations(a) 3.5 % NaCl solution; (b) 7 % NaCl solution; (c) 10 % NaCl solution

Figure 10 presents the potentiodynamic polarization curves of the 7.6 J-1 specimen in the above three concentrations of NaCl solutions. The results show that the self-corrosion potential of this specimen decreased with the increase of NaCl concentration, which was the highest in 3.5 % NaCl solution and the lowest in 10 % NaCl solution. Combined with the experimental results in Figure 6, it can be concluded that the increase of Cl^- concentration generally reduces the corrosion resistance of 2Cr13 stainless steel.

 https://doi.org/10.64486/m.66.1.13

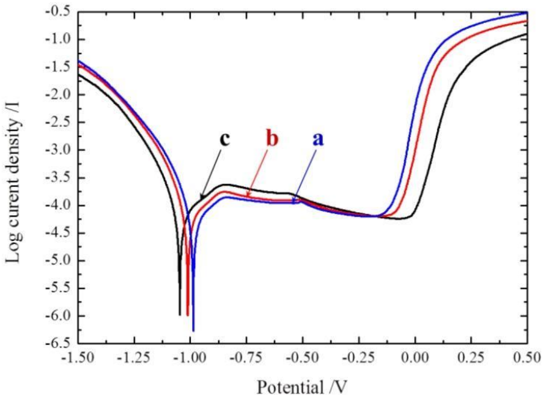

Figure 10. Polarization curves of unpeened specimen in NaCl solutions with different concentrations(a) 3.5 % NaCl solution; (b) 7 % NaCl solution; (c) 10 % NaCl solution

The Nyquist plots of different specimens in 3.5 % NaCl solution are shown in Figure 11. The impedance spectra of all specimens showed a single capacitive arc, and a larger capacitive arc radius indicates a larger charge transfer resistance and better corrosion resistance. The results show that the capacitive arc radii of laser shock peened specimens were significantly larger than that of the unpeened specimen, and the capacitive arc radius of LSP-2 specimen was larger than that of LSP-1 specimen, which was in turn larger than that of 5.6 J-1 specimen, consistent with the polarization curve analysis results.

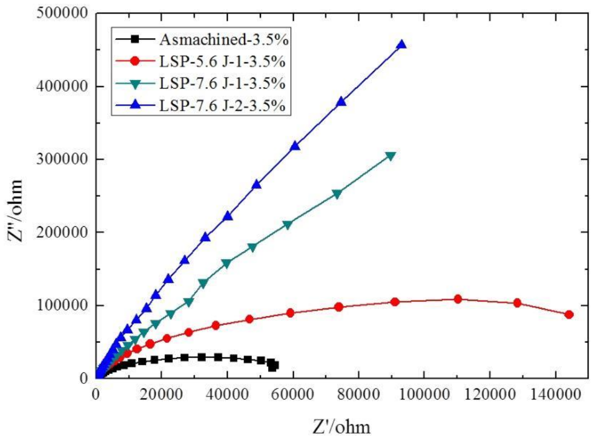

Figure 11. Nyquist plots of as-machined and different LSPed specimens in 3.5 % NaCl solution.

Figure 12 shows the electrochemical impedance spectroscopy (EIS) curves of the untreated 2Cr13 stainless steel specimens in NaCl solutions with different mass fractions. The results indicate that the impedance arc radius of the specimens was the largest in 3.5 % NaCl solution. With the increase of NaCl concentration, the impedance arc radius decreased significantly, and the impedance arc radius in 10 % NaCl solution was smaller than that in 7 % NaCl solution. The above results confirm that the increase of Cl^- concentration leads to the gradual deterioration of the electrochemical corrosion resistance of 2Cr13 stainless steel.

https://doi.org/10.64486/m.66.1.13

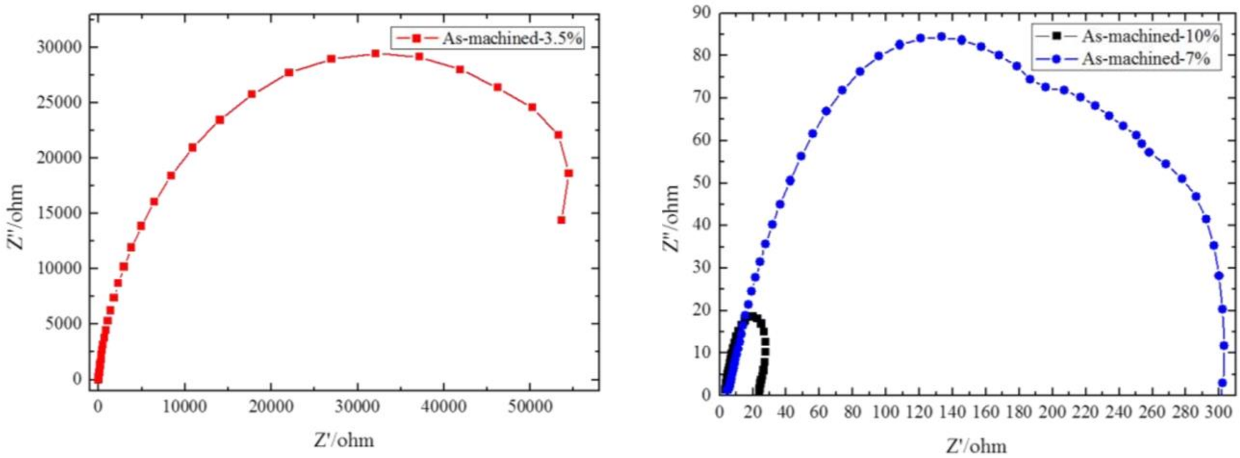

Figure 12. Nyquist plots of as-machined specimen in NaCl solution with different concentration

Figure 13 presents the electrochemical impedance spectroscopy (EIS) curves of the 7.6 J-1 specimen in NaCl solutions with different mass fractions. The results show that its variation trend is consistent with that of the untreated specimen: the impedance arc radius of the specimen is the largest in 3.5 % NaCl solution, followed by that in 7 % NaCl solution, and the smallest in 10 % NaCl solution. The above results indicate that with the increase of Cl^- concentration, the impedance arc radii of all specimens decrease significantly, and the electrochemical corrosion resistance gradually deteriorates.

By comparing the results in Figure 12, it can be seen that after laser shock peening (LSP) treatment, the reduction amplitude of the impedance arc radius of the treated specimen with the increase of NaCl concentration is significantly lower than that of the untreated specimen, indicating that LSP treatment can significantly improve the stability of the corrosion resistance of 2Cr13 stainless steel. The improved electrochemical corrosion resistance can slow down the pitting and intergranular corrosion damage of component surfaces in outdoor rain and salt spray environments, reduce the degradation rate of surface quality and dimensional accuracy during long-term service, and maintain the transmission accuracy and stability of the piano action mechanism for a longer period.

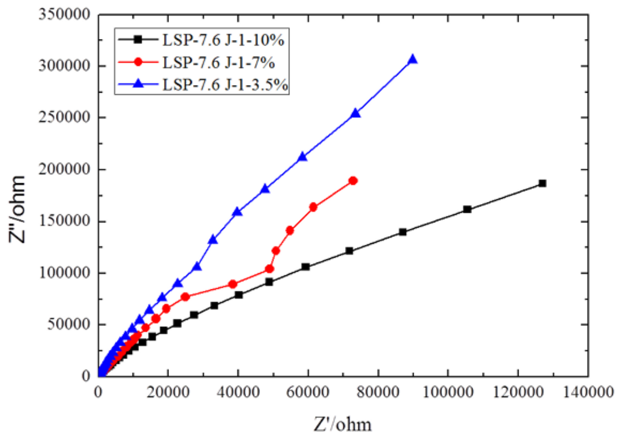

Figure 13. Nyquist plots of 7.6 J-1 specimen in NaCl solution with different concentration.

4. Conclusions

In this paper, the effect of laser shock peening process on the corrosion resistance of 2Cr13 stainless steel for outdoor pianos was systematically studied, and the following main conclusions were drawn:

1. Laser shock peening can significantly refine the surface martensite laths of 2Cr13 stainless steel, producing high-density dislocations and nano-precipitates. The microhardness increases with the

https://doi.org/10.64486/m.66.1.13

increase of peening layers, with a maximum improvement of 44.1 %, which can significantly improve the wear resistance and deformation resistance of outdoor piano components.

2. Laser shock peening significantly improved the corrosion fatigue resistance of 2Cr13 stainless steel. With pH values of 3, 7 and 11, the corrosion fatigue life of 7.6 J laser shock peened specimen increased by 9.69 %, 15.08 % and 8.38 %, respectively. The effective action area of laser shock peening is mainly concentrated at the crack tip, and the residual compressive stress is gradually released with crack propagation.
3. Laser shock peening improved the electrochemical corrosion resistance of 2Cr13 stainless steel. In 3.5 % NaCl solution, the self-corrosion current density of the 2-layer peened specimen decreased by 42.3 %. The corrosion resistance increases with the increase of peening energy and layer number, and decreases with the increase of Cl^- concentration. This result provides experimental support for the anti-corrosion design of outdoor piano components in different outdoor environments.

References

1. L. Soufeiani, G. Foliente, K. T. Q. Nguyen, et al., "Corrosion protection of steel elements in facade systems–a review," *Journal of Building Engineering*, vol. 32, p. 101759, 2020. https://doi.org/10.1016/j.jobe.2020.101759
2. P. Zamani, Z. Valef, and K. Jafarzadeh, "Comprehensive study on corrosion protection properties of Al_2O_3, Cr_2O_3 and Al_2O_3-Cr_2O_3 ceramic coatings deposited by plasma spraying on carbon steel," *Ceramics International*, vol. 48, no. 2, pp. 1574–1588, 2022. https://doi.org/10.1016/j.ceramint.2021.09.237
3. X. Q. Zhu, Q. X. Dai, M. Zhou, et al., "Effect of tempering temperature on stress-corrosion cracking and mechanical hysteresis of 2Cr13 stainless steel," *Transactions of Nonferrous Metals Society of China*, vol. 19, suppl. 1, pp. 11–13, 2009. https://doi.org/10.1016/S1003-6326(09)60084-4
4. M. Topic, C. Allen, and R. Tait, "The effect of cold work and heat treatment on the fatigue behaviour of 3CR12 corrosion resistant steel wire," *International Journal of Fatigue*, vol. 29, no. 1, pp. 49–56, 2007. https://doi.org/10.1016/j.ijfatigue.2006.02.050
5. M. Maher, I. Iraola-Arregui, H. B. Youcef, et al., "The synergistic effect of wear-corrosion in stainless steels: A review," *Materials Today*: Proceedings, vol. 45, pt. 5, pp. 2583–2588, 2021. https://doi.org/10.1016/j.matpr.2021.05.010
6. R. Sundar, P. Ganesh, R. K. Gupta, et al., "Laser shock peening and its applications: A review," Lasers in Manufacturing and *Materials Processing*, vol. 6, no. 4, pp. 327–368, 2019. https://doi.org/10.1007/s40516-019-00098-8
7. X. Wei, C. Zhang, and X. Ling, "Effects of laser shock processing on corrosion resistance of AISI 304 stainless steel in acid chloride solution," *Journal of Alloys and Compounds*, vol. 723, pp. 237–242, 2017. https://doi.org/10.1016/j.jallcom.2017.06.283
8. J. Z. Lu, H. Qi, K. Y. Luo, et al., "Corrosion behaviour of AISI 304 stainless steel subjected to massive laser shock peening impacts with different pulse energies," *Corrosion Science*, vol. 80, pp. 53–59, 2014. https://doi.org/10.1016/j.corsci.2013.11.003
9. M. Nataraj and S. Swaroop, "Effect of laser peening without coating on mechanical and microstructural behaviour of SS 304 stainless steel," *Materials Today Communications*, vol. 33, p. 104200, 2022. https://doi.org/10.1016/j.mtcomm.2022.104200
10. D. Liu, Y. Shi, J. Liu, et al., "Effect of laser shock peening on corrosion resistance of 316L stainless steel laser welded joint," Surface and Coatings Technology, vol. 378, p. 124977, 2019. https://doi.org/10.1016/j.surfcoat.2019.07.048
11. Z. Y. Li, X. W. Guo, and Z. B. Yu, "Influence of laser shock peening on surface characteristics and corrosion behavior of zirconium alloy," *Materials Characterization*, vol. 206, p. 113387, 2023. https://doi.org/10.1016/j.matchar.2023.113387
12. B. O. Okonkwo, J. Peng, H. Lin, et al., "A comparative study of the long-term corrosion behavior of two different 304 stainless steels in boron-lithium containing high temperature water," *Electrochimica Acta*, vol. 538, p. 147010, 2025. https://doi.org/10.1016/j.electacta.2025.147010
13. S. Choudhary, R. G. Kelly, and N. Birbilis, "On the origin of passive film breakdown and metastable pitting for stainless steel 316L," *Corrosion Science*, vol. 230, p. 111911, 2024. https://doi.org/10.1016/j.corsci.2024.111911

14. K. Y. Luo, Y. F. Yin, C. Y. Wang, et al., "Effects of laser shock peening with different coverage layers on fatigue behaviour and fractural morphology of Fe-Cr alloy in NaCl solution," *Journal of Alloys and Compounds*, vol. 773, pp. 168–179, 2019. https://doi.org/10.1016/j.jallcom.2018.09.147
15. W. Deng, C. Wang, H. Lu, et al., "Fatigue crack initiation and growth of laser shock peened 2Cr13 martensitic stainless steel as a function of the coverage layer," *International Journal of Fatigue*, vol. 175, p. 107792, 2023. https://doi.org/10.1016/j.ijfatigue.2023.107792
16. C. Wang, K. Luo, X. Bu, et al., "Laser shock peening-induced surface gradient stress distribution and extension mechanism in corrosion fatigue life of AISI 420 stainless steel," *Corrosion Science*, vol. 177, p. 109027, 2020. https://doi.org/10.1016/j.corsci.2020.109027
17. Y. Sheng, A. Feng, X. Cao, et al., "Effects of laser non-uniform shock peening on the microstructure and fatigue performance of SUS 304 stainless steel welded joints," *Materials Science and Engineering A*, vol. 898, p. 146287, 2024. https://doi.org/10.1016/j.msea.2024.146287
18. C. Rubio-Gonzalez, C. Felix-Martinez, G. Gomez-Rosas, et al., "Effect of laser shock processing on fatigue crack growth of duplex stainless steel," *Materials Science and Engineering A*, vol. 528, no. 3, pp. 914–919, 2011. https://doi.org/10.1016/j.msea.2010.10.020
19. Y. Liao, C. Ye, H. Gao, et al., "Dislocation pinning effects induced by nano-precipitates during warm laser shock peening: Dislocation dynamic simulation and experiments," *Journal of Applied Physics*, vol. 110, no. 2, p. 023518, 2011. https://doi.org/10.1063/1.3609072
20. M. Zhuang, L. Y. Hong, and W. Cheng, "Investigation of laser shock peening on aero-engine compressor rotor blade," *Key Engineering Materials*, vols. 373–374, pp. 404–407, 2008. https://doi.org/10.4028/www.scientific.net/KEM.373-374.404